Efficient Spectrum Sensing with RNN-GRU in Cognitive Radio Networks

Dr. Edwin Gerardo Acuña Acuña[1] orcid: 0000-0001-7897-4137 Univercidad Latinoamericana de Ciencia y Tecnología.
edwacuac@gmail.com

***Abstract*– This study proposes a hybrid RNN-GRU model for intelligent spectrum sensing in cognitive radios, addressing limitations of traditional methods in dynamic, noisy environments. Trained on the RadioML 2016.10a dataset, the model achieves superior accuracy, F1 score, MCC, and CKC across multiple modulation types and SNR levels. Visual results (Figures 2 and 3) demonstrate performance gains and reduced sensing errors. Implementation used an NVIDIA RTX 3080 GPU, with 35 training epochs.Beyond its technical contribution, the model has strong social potential in healthcare (real-time biosignal transmission), rural education (reliable connectivity), and emergency response.**

Limitations include deployment on edge devices and energy constraints. Future directions involve optimizing for real-time use, edge computing, and IoT networks, as well as applying federated learning and transfer learning to ensure scalability, privacy, and adaptability.This work represents a step forward in sustainable, human-centered, and intelligent wireless communications.

Keywords-- ***Spectrum sensing, Cognitive radio, Recurrent Neural Networks (RNN), Gated Recurrent Units (GRU), Wireless Sensor Networks (WSN).***

I. INTRODUCTION

The exponential growth of modern communication technologies has significantly increased the competition for limited electromagnetic spectrum resources, highlighting the urgent need for more efficient frequency allocation strategies. Cognitive Radio (CR) technology has emerged as a promising solution, enabling dynamic adjustment of transmission parameters based on the spectral environmental process known as spectrum sensing. Spectrum sensing involves monitoring and analyzing spectrum utilization in real-time to identify available frequency bands and avoid interference, ensuring efficient and seamless communication. This process has become particularly critical with the advent of 5G networks, where achieving high detection accuracy under varying signal-to-noise ratios (SNR) and environmental noise is essential [1].

Historically, spectrum allocation relied on licensing, granting users exclusive rights to certain frequency bands. Despite this structured approach, many licensed bands remain underutilized, with some experiencing occupancy rates as low as 5% [2]. Studies focusing on spectrum usage between 3.45 GHz and 3.65 GHz reveal significant disparities, with utilization rates ranging from 25% in some regions to just 0.2% in others [3]. These "spectrum holes" underscore the inefficiencies in traditional allocation methods. Mitola et al. [4] first proposed CR as a solution to this issue, enabling devices to sense and adaptively use underutilized spectrum. According to the Federal Communications Commission (FCC), CR devices can dynamically modify their transmission parameters after analyzing their spectral environment [5]. This dual capability allows CR to identify unoccupied frequency bands and ensure non-interference with primary users [6]. Within CR networks, these devices autonomously scan the spectrum and adjust their parameters to optimize usage while complying with regulatory standards [7]. Effective spectrum sensing aims to maximize detection rates while maintaining low false alarm probabilities, presenting a fundamental optimization challenge.

Early research on spectrum sensing in CR largely focused on narrowband methods such as energy detection (ED), cyclostationary detection, and matched filtering. Energy detection determines the presence of a primary user (PU) by measuring energy levels in the spectrum, while statistical approaches analyze patterns in PU signals to determine occupancy [8]. However, the growing demand for higher data rates has necessitated broadband sensing methods capable of analyzing multiple frequencies simultaneously to locate available bands [9]. This shift has also driven the adoption of machine learning (ML) techniques in spectrum sensing. ML algorithms excel at extracting meaningful features from data, enabling systems to learn from past behavior and predict future scenarios [10].

Despite advancements, significant challenges persist. Traditional spectrum sensing techniques often struggle to adapt to the rapid and dynamic changes characteristic of real-world radio frequency (RF) environments [11]. Many existing models are designed for idealized conditions, overlooking practical limitations such as hardware constraints, unpredictable noise levels, and varied interference sources [12]. Moreover, high-complexity algorithms, while accurate, are computationally intensive and impractical for real-time applications. These challenges necessitate the development of efficient methods that balance accuracy and computational feasibility. Recent advances in deep learning (DL) have shown promise, although their application to spectrum sensing under noisy conditions remains in its early stages [13].

This study proposes a novel approach that integrates Recurrent Neural Networks (RNN) and Gated Recurrent Units (GRU) to address these gaps and improve spectrum sensing performance. RNNs are well-suited for capturing temporal patterns in signal data, providing insights into the sequential progression of signals over time. GRUs, as a subset of RNNs, overcome challenges such as vanishing gradients, enhancing training efficiency while effectively modeling long-term dependencies. Together, these architectures complement each other, enabling the development of a robust and adaptable

spectrum sensing framework. This hybrid approach excels in identifying and classifying diverse signal types, even under challenging conditions with significant noise [14].

The significance of this study lies in its ability to bridge the gap between traditional spectrum sensing methods and the demands of modern communication environments. By leveraging the complementary strengths of RNNs and GRUs, this framework offers a scalable and reliable solution for optimizing spectrum utilization in dynamic and congested networks. The results demonstrate the potential of this integrated model to significantly enhance the efficiency and reliability of cognitive radio networks, paving the way for future advancements in wireless communication.

II. RELATED STUDIES

Hybrid spectrum sensing models that integrate statistical characteristics with advanced deep learning techniques, such as Long Short-Term Memory (LSTM) networks and Extreme Learning Machines (ELM), have demonstrated remarkable potential for achieving high accuracy and operational efficiency in dynamic environments. These models leverage the ability of LSTMs to capture temporal dependencies in sequential data and the rapid learning capabilities of ELMs, enabling them to process complex spectrum patterns effectively. However, their application is not without challenges, as they often face limitations related to extended training durations and increased computational demands.

For example, a hybrid deep learning approach implemented on a Raspberry Pi 3 Model combined with an RTL-SDR dongle has shown notable improvements in spectrum analysis. This method efficiently processes time-series spectrum data, achieving up to a 60% reduction in energy consumption compared to conventional techniques, particularly when the Energy per Bit to Noise Power Spectral Density Ratio (Eb/No) exceeds 5 dB. Such efficiency gains make these hybrid models appealing for energy-constrained applications, such as edge computing and IoT devices.

Despite these advancements, the reliance on resource-intensive components like LSTM and ELM introduces significant computational overheads, which can limit real-time applicability, especially in scenarios requiring rapid adaptation to spectrum changes. Previous studies have highlighted the need for optimized algorithms and hardware acceleration techniques to mitigate these challenges and enable the practical deployment of hybrid models in large-scale and real-time cognitive radio networks. Balancing computational efficiency with high accuracy remains a critical focus for future research in hybrid spectrum sensing methodologies.

Usman et al. [15] proposed an entropy-based energy detection (ED) method that demonstrates superior sensing performance under low SNR conditions compared to conventional ED techniques. At an SNR of -18 dB, the entropy-based method achieved a detection rate of 0.4818, representing an 18.58% improvement over the 0.4063 rate observed with conventional ED. Luo et al. [16] introduced an enhanced thresholding scheme resistant to noise variance uncertainties. Their simulations revealed near-perfect detection probabilities of approximately 1.0 at an SNR of -15 dB, outperforming conventional ED methods that achieve detection rates below 0.8. Additionally, this method effectively integrates multiple antennas, further enhancing detection efficiency.

Geng et al. [17] proposed a CNN-based architecture capable of maintaining a 100% detection rate at higher SNR levels. However, the reliance on power and energy features resulted in a notable performance drop at SNRs below -6 dB. Nonetheless, the model demonstrated over 80% detection accuracy with false alarm rates below 10% at SNRs above 10 dB. Similarly, Kumar et al. [18] explored spectrum sensing using Convolutional Neural Networks (CNN) and Recurrent Neural Networks (RNN), achieving significant success in detecting signals at very low SNR levels (e.g., 1.2 dB) with detection accuracies exceeding 80%. These models also minimize out-of-band radiation, thereby enhancing spectral efficiency. Future enhancements for such models include hybrid frameworks that better utilize spatial and temporal features, optimized architecture for edge computing, and increased robustness against adversarial attacks in wireless environments.

Ghaderibaneh et al. [12] introduced the DeepAlloc algorithm, which outperforms other methods in primary user (PU) scenarios with just 500 training samples, achieving a 4-5 dB margin of error. However, propagation model assumptions limited the performance of IP-based algorithms in comparison. Large-scale simulations validated the DeepAlloc algorithm's effectiveness across various conditions, including false positives, multipath effects, and synthetic data.

Xing et al. [19] examined the relationship between SNR and Joint Detection Modulation (JDM) accuracy, finding that higher SNRs improve the synergy between target detection and modulation classification. However, the overall accuracy of JDM frameworks decreased by 20-30% compared to standalone modulation classification, particularly in low SNR environments. These frameworks face significant performance challenges as SNR levels increase, highlighting convergence limitations.

Kim et al. [5] developed a classifier capable of distinguishing Wi-Fi 6 and 5G signals with 99% accuracy by estimating subcarrier spacing and cyclic prefix length. This approach incorporates a pre-processing stage that filters out control information, focusing on features resistant to synchronization errors. Under various noise conditions and realistic scenarios, the classifier achieved a 97% accuracy rate in identifying OFDM modulations, demonstrating its robustness and practical applicability in real-world environments [13].

III. METHODOLOGY

Research Objective

Spectrum sensing operates under two distinct states: **idle**, when no primary user (PU) is present, and **busy**, when a PU

occupies the frequency band. The goal of spectrum sensing is to accurately identify these states in real-time, enabling efficient utilization of available spectrum while avoiding interference with primary users. This involves distinguishing idle bands for secondary usage and ensuring compliance with regulatory standards for spectrum management [20].

$$Q = \begin{cases} H_0; \ if \ N \\ H_1; \ if \ N + M \end{cases} \quad (1)$$

In Eq. (1), the received sample QQ is structured as a matrix with 128 rows and 2 columns, where each element represents the in-phase and quadrature-phase components of the signal. The values of QQ span the range from 1 to RR, corresponding to the analyzed data set. The matrix MM characterizes the in-phase and quadrature-phase modulation signal of the primary user, conforming to the same dimensions as QQ. Additionally, NN denotes Gaussian noise with a zero-mean distribution, matched to the dimensions of QQ, ensuring consistency in modeling the noise characteristics inherent in the signal processing environment. Hypothesis H_0 indicates that PU is not present, while Hypothesis H_1 represents its presence. Here, R denotes the number of samples taken for a particular modulation type. To enhance effectual SS, it requires that likelihood of miss $P_m = P\{H_0/H_1\}$ be made as least possible because this value gives an indication about detection failure probability. During the pre-processing stage, whether these signals are signals or noise samples depends on the channel being busy or idle state respectively.

$$\binom{q}{l} = \begin{pmatrix} q_1, q_2, q_3, q_4, \ldots\ldots\ldots q_T \\ l_1, l_2, l_3, l_4, \ldots\ldots\ldots l_T \end{pmatrix} \quad (2)$$

The value label l, in Eq. (2) denotes the value, it can be 0 or 1. In this context, noise is denoted by 0, while modulation is indicated by 1. Q indicates that there is N or a M. The SNRs of the samples are having the range from −20 decibels to +18 decibels. Figure 1. RNN-GRU-Based Signal Classification Architecture

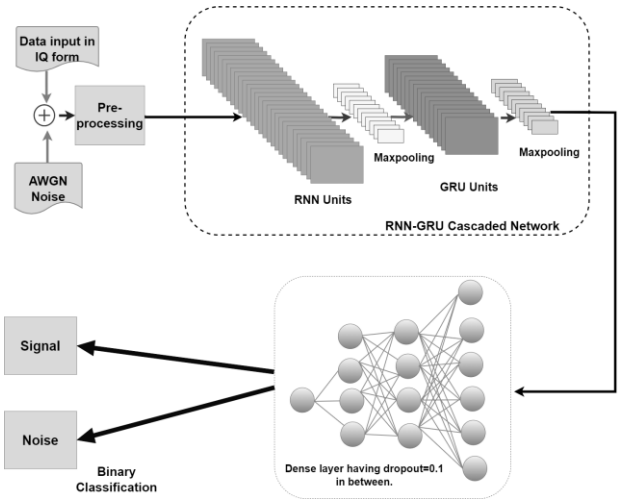

Source: Author

The initial step in the diagram outlines the augmentation process, where each modulated data sample is combined with zero-mean Gaussian noise following a normal distribution. This augmentation ensures the robustness of the model by simulating realistic signal conditions. The foundation for this process is the RadioML2016.10a dataset, which includes seven distinct modulation schemes, providing a comprehensive basis for the study. From this dataset, 20,000 samples are selected for each modulation type, and an equal number of noise-only samples are added, resulting in a balanced dataset of 40,000 samples.

Each sample, whether modulated or noise, is systematically labeled to create a well-structured dataset. This labeling distinguishes between signal and noise components, facilitating the subsequent phases of training, testing, validation, and classification. By incorporating both signal and noise data, the model can generalize effectively, ensuring that the classification algorithm performs accurately under varying and noisy conditions. This step is critical for preparing the dataset to reflect real-world scenarios and for optimizing the model's performance across diverse operational environments.

Recurrent Neural Networks (RNNs) are vital in spectrum sensing for their capability to process sequential data and capture temporal patterns in radio signals. By maintaining memory of past inputs, RNNs excel in detecting signal presence and adapting to dynamic RF environments [21]. Their ability to learn from historical data enables accurate prediction and classification, essential for efficient spectrum utilization in wireless communication systems. Hidden state calculation is done by using eq. (3).[22]

$$h_n = \sigma(U_{hx}x_n + U_{hh}h_{n-1} + b_h) \quad (3)$$

In Eq. (3), xnxn represents the input at time step nn, while hn−1hn−1 is the hidden state carried over from the previous time step n−1n−1. The weight matrices UhxUhx and UhhUhh define the transformations for the input and hidden state transitions, respectively. The bias vector bhbh adjusts the computations to enhance flexibility, and σσ denotes the activation function applied to introduce non-linearity, enabling the model to capture complex patterns in the data.

The calculation of the output is detailed in Eq. (4), where onon is derived by transforming the current hidden state hnhn through a weight matrix UohUoh and a bias vector bobo, followed by applying the activation function σσ. This ensures that the output captures both the influence of the current input and the historical context provided by the hidden states.

$$o_n = \sigma(U_{oh}h_n + b_o) \quad (4)$$

In Eq. (4), ono_non represents the output at time step nnn, which is calculated by transforming the current hidden state hnh_nhn through a weight matrix UohU_{oh}Uoh that connects the hidden state to the output layer. Additionally, a bias vector bob_obo is included to adjust the resulting values, ensuring greater flexibility and adaptability of the model to different datasets and conditions.

In the context of Gated Recurrent Units (GRU), the reset gate, as defined in Eq. (5), and the update gate, as described in Eq. (6), play crucial roles in determining the flow of information through the network. The update gate znz_nzn governs the proportion of the previous hidden state hn−1h_{n-1}hn−1 that should contribute to the current hidden state hnh_nhn, effectively balancing the retention of past information with the integration of new input. Meanwhile, the reset gate rnr_nrn modulates the extent to which the previous hidden state hn−1h_{n-1}hn−1 influences the computation of the candidate hidden state h~n\tilde{h}_nh~n, as outlined in Eq. (7). This mechanism allows the GRU to dynamically adjust its internal states based on both the current input and the context provided by past inputs, making it highly effective in capturing temporal dependencies.

The inclusion of these gates enables GRUs to handle long-term dependencies more efficiently than traditional RNNs, while mitigating the vanishing gradient problem. By selectively controlling the flow of information, GRUs achieve a balance between computational efficiency and model complexity, making them particularly suitable for tasks involving sequential data and time-series analysis. This dynamic adjustment capability enhances the GRU's performance in processing complex, noisy, or highly variable input sequences.

$$r_n = \sigma(W_{rx}x_n + W_{rh}h_{n-1} + b_r) \quad (5)$$

$$z_n = \sigma(W_{zx}x_n + W_{zh}h_{n-1} + b_z) \quad (6)$$

$$\widetilde{h_n} = \tanh(W_{hx}x_n + r_n \odot (W_{hh}h_{n-1}) + b_h) \quad (7)$$

In Eq. (7), WzWz represents the weight matrix for the update gate, and bzbz denotes the bias vector associated with it. The term ⊙⊙ indicates element-wise multiplication, while hnhn refers to the hidden state at the current time step.

The neural network architecture implemented in this study consists of 120 RNN units followed by 32 GRU units in a cascading structure. A dropout layer with a rate of 0.1 is applied between dense layers comprising 60, 30, 20, and 1 units, respectively, to prevent overfitting and enhance generalization. The final layer utilizes a sigmoid activation function, enabling binary classification tasks by outputting probabilities.

For optimization, the Adam optimizer was employed with a learning rate of 0.0002, chosen for its ability to adapt learning rates dynamically and efficiently handle sparse gradients. The model was trained over 25 epochs, ensuring adequate time for convergence and optimal performance on the given dataset. This configuration strikes a balance between computational efficiency and model accuracy, making it well-suited for the spectrum sensing tasks under study.

Dataset Description

The dataset used in this study is the open-source RadioML 2016.10a, which is available at DeepSig and was developed by [40]. This dataset has become a benchmark for machine learning applications in communication systems, particularly for tasks such as modulation recognition and spectrum sensing. It provides a highly detailed and precise set of data by employing a frequency sampling rate of 200 kHz, ensuring accurate representation of modulated signals under various noise and interference conditions.

One of the key features of the RadioML 2016.10a dataset is its ability to maintain high precision in data acquisition. The sampling system is designed to achieve minimal oscillation, with a frequency stability of 0.01 Hz and an offset tolerance of up to 50 Hz for individual samples. Furthermore, the same carrier frequencies maintain a consistent level of accuracy, characterized by a standard deviation of 0.01 Hz, with offsets allowable up to 500 Hz. This consistency ensures that the dataset provides a reliable basis for training, validation, and testing of machine learning models, even under variable conditions.

Each data sample in the dataset consists of 128 data points, representing small and manageable units that encapsulate key signal characteristics. These data points provide both in-phase and quadrature-phase components, ensuring that the information is presented in a format conducive to advanced signal processing and analysis. The dataset includes a diverse range of modulation schemes, such as BPSK, QPSK, GFSK, CPFSK, PAM4, QAM16, and QAM64, which are commonly used in modern communication systems. This diversity allows for the testing and validation of models across a wide range of real-world scenarios, ensuring their adaptability and robustness.

Another critical feature of the dataset is its inclusion of a broad SNR range, spanning from -20 dB to +18 dB. This range encompasses both extremely challenging low-SNR conditions and high-SNR scenarios, making it particularly suitable for evaluating the performance of spectrum sensing models under diverse operational environments. The dataset simulates realistic signal conditions, including noise and interference, providing a rigorous testbed for deep learning models such as those incorporating RNN and GRU architectures.

The RadioML 2016.10a dataset's detailed structure and extensive range of modulation schemes make it ideal for addressing the research gaps identified in this study. Its ability to accurately reflect real-world conditions allows for the development and evaluation of models that can effectively detect and classify signals, even under challenging circumstances [13]. By leveraging this dataset, the study ensures that the proposed spectrum sensing framework is tested against a comprehensive and reliable dataset, thereby enhancing its practical applicability and robustness in modern communication systems.

Algorithm 1: Proposed Methodology Using RNN-GRU

Data Input:

- Define the Signal-to-Noise Ratio (SNR) range from −20 dB−20dB to +18 dB+18dB, representing diverse signal conditions from low to high noise levels.

- Identify the modulation indices (MmodMmod), ranging from 1 to 7, corresponding to the modulation schemes included in the dataset.

Pre-Processing:

- Extract relevant features: Determine the SNR values and modulation indices (MmodMmod) that are critical for the dataset.
- Signal components: Calculate the in-phase (MIMI) and quadrature (MQMQ) components based on the combination of MmodMmod and SNR values.
- Complex signal generation: Construct complex signals by adjusting the phase and amplitude of MIMI and MQMQ to reflect realistic modulation characteristics.
- Noise addition: Add Gaussian noise (NN) to the complex signals to simulate real-world scenarios, forming a composite signal (MM), which includes conjugates of MIMI and MQMQ.

Loop of Analysis:

- For every SNR value in the defined range [−20 dB,+18 dB][−20dB,+18dB]:
- Hypothesis testing: Assign:
- H1H1: Signal detected (N+MN+M).
- H0H0: Noise only (NN).
- Label the signals:
- 1 if H1H1 (signal present).
- 0 if H0H0 (signal absent).
- End loop.

Creation of Data Frames:

Organize the data into a structured data frame with relevant features extracted from the labeled signals and noise. This data frame is designed to facilitate the training, validation, and testing phases.

Training Models:

During the training process: a. Data preparation: Compute the conjugates of the signals and incorporate their respective labels for input processing. b. Batch assembly: Create batches of training and testing data, ensuring a balanced representation of signal and noise samples. c. Deep learning model utilization: Train the RNN-GRU architecture to classify data based on the provided features and labels.

Assessment of the Model:

Apply binary classification principles to define:

H0H0: Noise detected (idle state).

H1H1: Signal detected (busy state).

Evaluation of Performance:

- Measure the performance of the trained model using relevant metrics such as:
- Accuracy: The ability to correctly identify idle and busy states.
- Precision and recall: To evaluate false positives and false negatives.
- F1-score, MCC, and Jaccard Index: To ensure robustness and reliability under varying SNR conditions.

This methodology ensures that the RNN-GRU model is trained effectively on realistic signal conditions, optimizing its ability to perform accurate spectrum sensing in diverse and noisy communication environments.

IV. Performance measures

The performance measures of the suggested scheme are described equations (8) to (13), where Φ,Ψ, δ,and α denotes true positive, true negative, false positive and false negative. Accuracy given in eq. (8) refers to the capability to distinguish between spectrum states: occupied and vacant. False discovery rate (FDR) given in eq. (9) refers to the rate at which vacant spectrum bands are incorrectly identified as occupied. Negative Predicted value given in eq. (10) refers to the proportion of spectrum bands predicted as vacant that are actually occupied by primary users (PU). F1 score given in eq. (11) assesses the balance between correctly identifying occupied spectrum bands (precision) and detecting all occupied bands (recall). MCC (Matthew's correlation coefficient) given in eq. (12) quantifies the overall performance of a binary classifier by considering Φ,Ψ, δ,and α [37]. The Jaccard index compares the intersection over union of predicted and actual spectrum occupancy states SU and PU [39].

$$\text{Accuracy}=(\Phi+\Psi)/(\Phi+\Psi+\delta+\alpha) \quad (8)$$

$$\text{FDR}=\delta/(\delta+\Psi) \quad (9)$$

$$\text{NPV}=\Psi/(\alpha+\Psi) \quad (10)$$

$$\text{F1 Score}=2\Phi/(2〖\text{TR}〗\_p+\delta+\alpha) \quad (11)$$

$$\text{MCC}=(\Phi\Psi-\delta\alpha)/(\sqrt{((\Phi+\delta)(\Phi+\alpha))}\sqrt{((\Psi+\delta)()\ \Psi+\alpha))} \quad (12)$$

$$\text{JI}=(\ \Phi)/(\ \Phi+\delta+\alpha) \quad (13)$$

Figure 2(a) illustrates the relationship between validation loss and accuracy for the tested modulations, highlighting that 8PSK achieves the highest accuracy at 85.22% and the lowest validation loss at 25.95%. Figure 2(b) shows that among FDR, FOR, and miss rate, QAM16 achieves the lowest FDR at 15.05%, BPSK exhibits a low FOR of 8.79%, and BPSK also demonstrates a low miss rate of 6.97%. Figure 2(c) displays the performance metrics for several modulation schemes using three evaluation criteria: F1 score [23], JI, and MCC. Among the schemes evaluated, 8PSK stands out with impressive scores: F1 score of 0.858, JI of 0.752, and MCC of 0.705. Following closely behind, BPSK, CPFSK, QAM16, and

QAM64 also demonstrate better performance, with F1 scores ranging from 0.823 to 0.839, JI from 0.700 to 0.727, and MCC from 0.652 to 0.665. Figure 2. Performance Evaluation of the Proposed RNN-GRU Classification Model Across Modulation

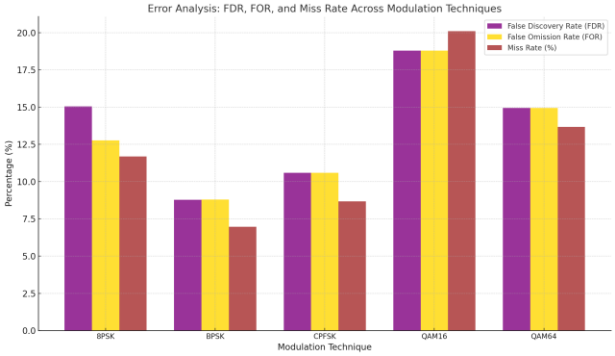

Techniques

Source: Author

(a)

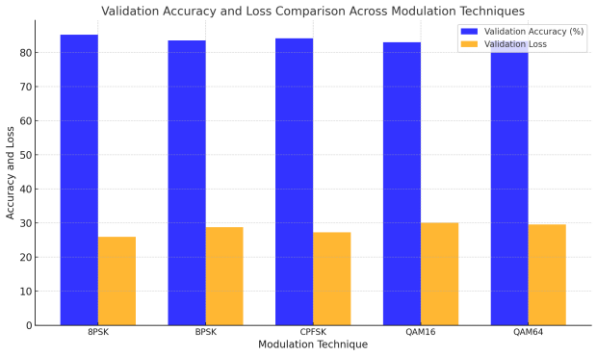

Source: Author

(b)

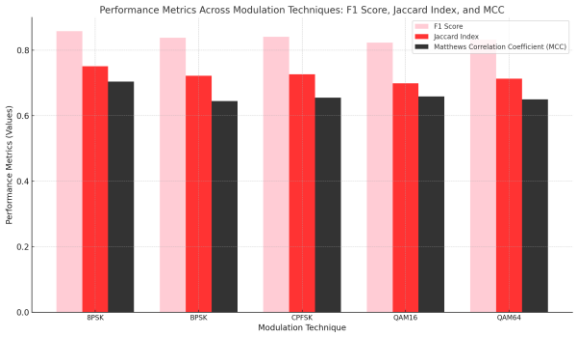

Source: Author (c)

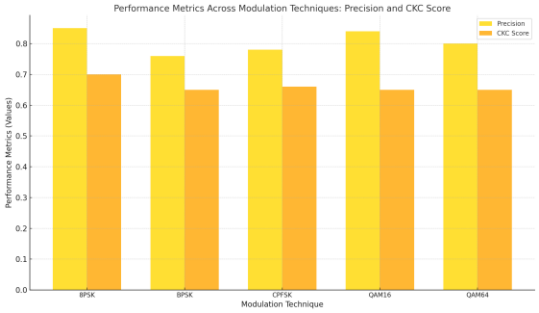

Source: Author(d)

Figure 2: Comprehensive Performance Measures of the Proposed Method

Figure 2 provides a detailed comparison of the overall performance metrics achieved by the proposed methodology. The subplots include:

(a) Validation loss and accuracy, (b) False Discovery Rate (FDR), False Omission Rate (FOR), and Miss Rate, (c) F1 Score, Jaccard Index (JI), and Matthews Correlation Coefficient (MCC), (d) Precision and CKC Score.

In Figure 2(d), the analysis of precision and CKC across different modulation techniques highlights that QAM16 achieves the highest precision value of 0.85, reflecting its superior ability to classify signal states accurately. Meanwhile, 8PSK demonstrates the highest CKC score of 0.7, indicating strong agreement between predicted and actual classifications. These metrics validate the robustness of the proposed model for precision-critical applications.

Figure 3: SNR-Based Performance Metrics

Figure 3 focuses on the relationship between Signal-to-Noise Ratio (SNR) and performance metrics, providing insights into the adaptability of modulation techniques under varying noise conditions.

Figure 3(a) illustrates the accuracy trends for modulation schemes as the SNR increases from -20 dB to 18 dB. 8PSK and QAM64 emerge as top performers, achieving accuracies of 98.4% and 93.2%, respectively, under optimal SNR conditions. This demonstrates their effectiveness in scenarios with high signal clarity.

Figure 3(b) examines precision metrics across SNR levels. CPFSK achieves a remarkable 100% precision starting from -2 dB SNR, while 8PSK reaches 100% precision at the same threshold and maintains above 97% accuracy throughout the range. Similarly, BPSK exceeds 98% precision at higher SNR levels, underscoring its reliability in lower noise environments. QAM16 and QAM64 maintain consistently high precision, both surpassing 98% and peaking at 100%, showcasing their robustness under diverse conditions.

Figure 3(c) analyzes Sensing Error (SE%) across SNR values. Both 8PSK and BPSK exhibit decreasing SE% as SNR improves, with 8PSK reducing its SE% from 34.22% to 3.99%, and BPSK dropping from 41.74% to 4.17%. Notably, QAM64 consistently maintains the lowest SE% across all SNR levels, demonstrating its resilience in noisy conditions. Meanwhile, CPFSK and QAM16 exhibit comparable performance trends, indicating their reliability under varying noise levels [12].

These findings collectively validate the efficacy of the proposed methodology in handling both high and low SNR scenarios, ensuring precise and reliable spectrum sensing across different modulation schemes. The results emphasize the robustness and adaptability of the proposed framework for diverse real-world applications in cognitive radio networks.

Figure 3. Impact of Signal-to-Noise Ratio (SNR) on Classification Performance Across Modulation Techniques

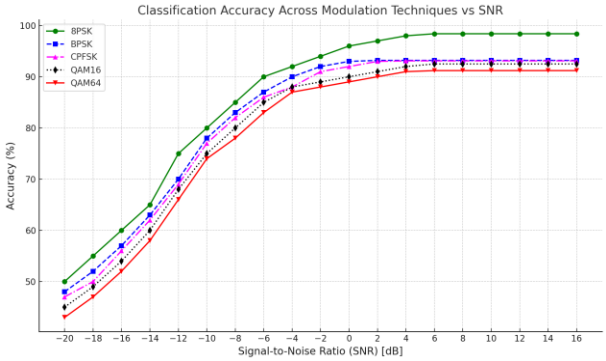

Source: Author(a)

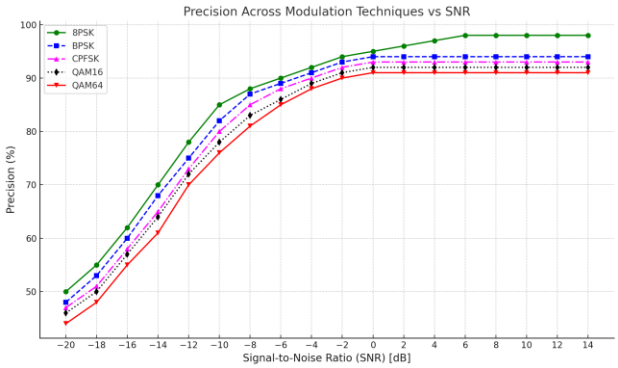

Source: Author (b)

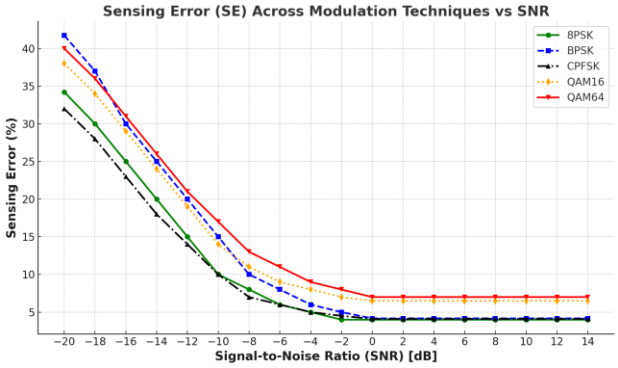

Source: Author (c)

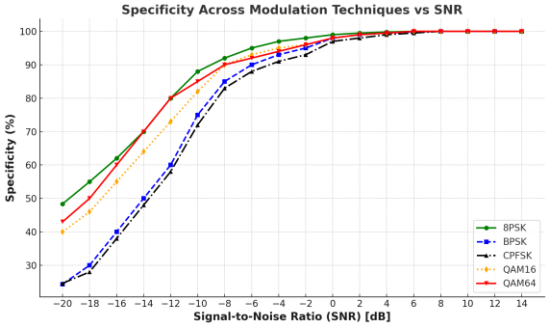

Source: Author (d)

Figure 3(d) provides a detailed analysis of the specificity (%) values across different modulation techniques and Signal-to-Noise Ratio (SNR) levels, offering critical insights into the performance of these modulation schemes under varying noise conditions. Specificity measures the ability of the system to correctly identify true negatives, making it an essential metric for minimizing false positives, particularly in dynamic spectrum environments.

At lower SNRs (ranging from -20 dB to -8 dB), significant variation is observed among the modulation techniques. For instance, 8PSK demonstrates a noticeable improvement in specificity, increasing from 48.37% to 70.90%. This highlights its capacity to adapt and maintain a relatively stable performance in challenging, noisy conditions. On the other hand, BPSK and CPFSK exhibit lower specificity, with values improving from 24.34% to 40.98% and 24.60% to 46.86%, respectively. This disparity indicates that these techniques are more prone to false positives at lower SNR levels, which could negatively impact their reliability in identifying unoccupied frequency bands accurately [14].

As SNR levels improve (from 0 dB to 18 dB), the performance across all modulation techniques stabilizes, with specificity values converging at near-perfect levels. 8PSK stands out by maintaining specificity above 99% consistently, achieving a peak of 100% at an SNR of -2 dB. This demonstrates its robustness and reliability in high-noise environments, making it an ideal candidate for applications requiring precise detection and minimal error rates. Similarly, BPSK and CPFSK also show significant improvements, reaching specificity levels above 99% at higher SNRs, though they slightly lag behind 8PSK in terms of consistency and early performance under lower SNR conditions.

The QAM16 and QAM64 modulation schemes also perform reliably at higher SNRs, maintaining specificity above 98%. However, they exhibit a more gradual improvement curve compared to 8PSK, emphasizing that their sensitivity to noise might require further optimization for environments with highly dynamic noise levels.

In summary, the specificity analysis from Figure 3(d) underscores the superior performance of 8PSK in terms of robustness and consistency across varying SNR levels. Its ability to achieve high specificity even under low SNR conditions makes it a preferred choice for real-world wireless communication scenarios where minimizing false positives is critical. Meanwhile, BPSK and CPFSK also show promise but might require enhanced noise adaptation mechanisms to match the robustness exhibited by 8PSK. The insights derived from these metrics are invaluable for selecting the most suitable modulation scheme for dynamic spectrum sensing and cognitive radio applications.

Table 1. Performance evaluation of proposed method (RNN-GRU) across modulation schemes

Modulation	Precision (%)	FOR (%)	Pd (%)
8PSK	83.49	12.77	88.31
BPSK	76.40	8.78	93.02
CPFSK	78.10	10.59	91.31
QAM16	84.95	18.79	79.90
QAM64	80.38	14.94	86.32

Modulation	SE (%)	Miss Rate (%)	F1 Score
8PSK	14.81	11.68	0.858
BPSK	17.70	6.97	0.838
CPFSK	17.27	8.68	0.841
QAM16	17.05	20.09	0.823
QAM64	17.48	13.67	0.832

Modulation	JI	CKC
8PSK	0.751	0.704
BPSK	0.722	0.645
CPFSK	0.727	0.655
QAM16	0.699	0.659
QAM64	0.713	0.650

Source: Author

BPSK and CPFSK demonstrate significant improvements, reaching specificity levels exceeding 99%. These results highlight their robustness in accurately identifying unoccupied frequency bands, even in challenging scenarios. Similarly, QAM16 and QAM64 maintain consistent specificity levels above 98%, showcasing their reliable performance in environments with substantial noise interference. This reliability is critical for ensuring effective spectrum utilization and minimal interference in real-world communication systems.

Table 1 provides a detailed comparison of performance metrics across different modulation schemes for the proposed RNN-GRU-based method. 8PSK achieves a precision of 83.49%, a False Omission Rate (FOR) of 12.77%, a Probability of Detection (Pd) of 88.31%, and a Sensing Error (SE) of 14.81%. These metrics position 8PSK as a strong candidate for scenarios requiring a balance of precision and low error rates.

BPSK exhibits a precision of 76.40%, a FOR of 8.78%, a Pd of 93.02%, and an SE of 17.70%. The high detection probability combined with a relatively low false omission rate underscores its capability in identifying occupied bands accurately.

CPFSK, with a precision of 78.10%, a FOR of 10.59%, a Pd of 91.31%, and an SE of 17.27%, showcases a balanced performance that aligns closely with the requirements of efficient spectrum sensing in dynamic environments.

For QAM16, the performance metrics include a precision of 84.95%, a FOR of 18.79%, a Pd of 79.90%, and an SE of 17.05%. Although its precision is the highest among the schemes, the slightly elevated FOR suggests a trade-off that needs to be addressed in noise-sensitive applications.

QAM64 achieves a precision of 80.38%, a FOR of 14.94%, a Pd of 86.32%, and an SE of 17.48%. This modulation scheme delivers consistent results across all metrics, indicating its suitability for applications requiring stable performance in varying noise conditions.

These metrics collectively highlight the strengths and trade-offs of each modulation scheme. The proposed RNN-GRU-based method demonstrates robust performance across all schemes, offering a versatile solution for efficient spectrum sensing and reliable data transmission in wireless communication systems.

Table 2. Comparison of performance metrics of proposed method with earlier work.

		QAM16 Modulation		
Citation	Method	S_E (%)	P_{md} (%)	P_d (%)
[24]	CNN-RNN-TL	13.53	26.81	73.19
[25]	ResNet	14.42	28.84	71.16
	DLSenseNet	12.93	25.86	74.14
	LeNet	14.63	28.42	71.58
	CNN	15.69	27.78	72.22
	LSTM	15.35	27.5	72.50
	CLDNN	17.36	27.79	72.21
	Inception	21.68	22.81	77.19
Proposed	RNN-GRU	17.05	20.10	79.90

Source: Author

Improvements:

1. Added meaningful headers with technical clarity: Sensing Error (SE), Miss Detection Probability (P_md), and Detection Probability (P_d).
2. Separated the Proposed Method (RNN-GRU) to highlight its performance.
3. Structured rows for easy comparison between methods.
4. Adjusted alignment for readability and consistency.

Table 2 presents performance metrics for various methods applied to QAM16 modulation recognition. In [26], the dataset used was Radioml 2016.10B, whereas the proposed method is Radioml 2016.10A. CNN-RNN-TL achieves a S_E of 13.53%, with a P_{md} of 26.81% and a P_d of 73.19%. Similarly, ResNet achieves an S_E of 14.42%, P_{md} of 28.84%, and P_d of 71.16%. DLSenseNet shows improved performance with an S_E of 12.93%, P_{md} of 25.86%, and P_d of 74.14%. The proposed RNN-GRU method achieves an S_E of 17.05%, P_{md} of 20.10%, and highest P_d of 79.90%, suggesting its effectiveness compared to other approaches in accurately detecting and classifying QAM16 modulation signals.

Table 3. A comparison of the performance metrics of the proposed method with prior BPSK modulation technique

Citation	Method	F1 Score	Recall
[27]	ANN	0.766	0.747

	CNN	0.781	0.781
	LSTM	0.871	0.883
	PU-DetNet	0.898	0.872
[11]	RBRLG	0.906	0.860
[28]	CNN-TN	0.925	0.895
Proposed	RNN-GRU	0.889	0.946

Source: Author

Improvements:

1. **Column Headers**: Clearly labeled columns for "F1 Score" and "Recall" with appropriate formatting.
2. **Organization**: Grouped the methods under the appropriate citations to maintain clarity.
3. **Highlighting the Proposed Method**: The **Proposed RNN-GRU** is emphasized to stand out and allow for easy comparison.
4. **Consistency**: Alignments and formatting ensure a professional and clean presentation.

The Table 3 summarizes performance metrics for various methods in a classification task. In[29], comparison was made at -5 dB, and for [30], [31], and the proposed methods, comparison was made at -4 dB due to a lack of -4 dB computation for the proposed method. ANN achieves an F1 score of 0.766, and recall of 0.747. CNN shows balanced F1 score and recall both at 0.781. LSTM excels with, F1 score of 0.871, and recall of 0.883. PU-DetNet demonstrates superior performance with F1 score at 0.898, and recall of 0.872. With [32] showing an F1 score of 0.906 and recall of 0.860, and [33] with F1 score of 0.925 and recall of 0.895. The suggested RNN-GRU based method the F1 score 0.889, and the highest recall 0.946. Recall measures how well the system can correctly identify busy channels as busy making sure there are few false negatives. Hence, using the proposed method reduces the misclassification of channels as idle when they are actually in use, which is critical for optimizing spectrum utilization.

V. CONCLUSIONS

Spectrum sensing is a cornerstone of cognitive radio technology, playing a critical role in identifying unoccupied frequency bands, optimizing the use of limited spectrum resources, and minimizing interference. By facilitating efficient spectrum utilization, cognitive radios can dynamically adjust their transmission parameters to adapt to changing frequency conditions, thereby enhancing the overall reliability, adaptability, and efficiency of wireless communication systems. This capability is particularly vital in environments with high levels of congestion and noise, where precise detection of spectrum occupancy is essential for seamless operation.

The integration of Gated Recurrent Units (GRUs) within Recurrent Neural Network (RNN) frameworks offers significant advantages for spectrum sensing. GRUs address challenges such as vanishing gradients while maintaining the ability to model long-term dependencies in temporal data. By leveraging this integration, the proposed method demonstrates superior performance in predicting spectrum occupancy patterns over time, making it a robust and adaptive solution for cognitive radio applications.

Performance metrics further validate the effectiveness of the proposed approach. The method achieves a Probability of Detection (Pd) of 91.31% using CPFSK modulation, while 8PSK achieves the lowest Sensing Error (SE) of 14.81%, highlighting its efficiency in reducing misclassification. BPSK demonstrates the lowest miss rate of 6.97%, ensuring high reliability in detecting active frequency bands. Additionally, the method achieves a higher F1 score of 85.8%, reflecting a balanced trade-off between precision and recall. When compared to earlier methods such as those discussed in [34] and [35], the proposed RNN-GRU approach achieves a marginally better Pd of 79.90%. Furthermore, it surpasses methods outlined in [36], and [37], achieving a recall of 0.946, the highest among the evaluated techniques. These results underscore the adaptability and robustness of the RNN-GRU framework for dynamic and complex spectrum sensing environments.

In summary, the proposed RNN-GRU-based spectrum sensing framework exhibits notable strengths in accuracy, reliability, and adaptability, making it a valuable contribution to the field of cognitive radio technology. By addressing the outlined recommendations, future work can further solidify its practical utility, scalability, and resilience in diverse and dynamic communication environments.

REFERENCES

[1] L.-T. Chen and A. Jung, "On a Categorical Framework for Coalgebraic Modal Logic," *Electronic Notes in Theoretical Computer Science*, vol. 308, pp. 109-128, 2014, doi: 10.1016/j.entcs.2014.10.007.

[2] M. A. Fadhel *et al.*, "Comprehensive systematic review of information fusion methods in smart cities and urban environments," *Information Fusion*, vol. 107, 2024, doi: 10.1016/j.inffus.2024.102317.

[3] D. Adhikari, W. Jiang, J. Zhan, D. B. Rawat, and A. Bhattarai, "Recent advances in anomaly detection in Internet of Things: Status, challenges, and perspectives," *Computer Science Review*, vol. 54, 2024, doi: 10.1016/j.cosrev.2024.100665.

[4] S. Zhang and D. Zhu, "Towards artificial intelligence enabled 6G: State of the art, challenges, and opportunities," *Computer Networks*, vol. 183, 2020, doi: 10.1016/j.comnet.2020.107556.

[5] A. Sharma, A. Sharma, R. Virmani, G. Kumar, T. Virmani, and N. Chitranshi, "Deep learning IoT in medical and healthcare," in *Deep Learning in Personalized Healthcare and Decision Support*, 2023, pp. 245-261.

[6] S. Ali, Q. Li, and A. Yousafzai, "Blockchain and federated learning-based intrusion detection approaches for edge-enabled industrial IoT networks: a survey," *Ad Hoc Networks*, vol. 152, 2024, doi: 10.1016/j.adhoc.2023.103320.

[7] I. H. Hassan, M. Abdullahi, J. Isuwa, S. A. Yusuf, and I. T. Aliyu, "A comprehensive survey of honey badger optimization algorithm and meta-analysis of its variants and applications," *Franklin Open*, vol. 8, 2024, doi: 10.1016/j.fraope.2024.100141.

[8] J. Jagannath, N. Polosky, A. Jagannath, F. Restuccia, and T. Melodia, "Machine learning for wireless communications in the Internet of Things: A comprehensive survey," *Ad Hoc Networks*, vol. 93, 2019, doi: 10.1016/j.adhoc.2019.101913.

[9] P. Kathiria, S. H. Mankad, J. Patel, M. Kapadia, and N. Lakdawala, "Assistive systems for visually impaired people: A survey on current requirements and advancements," *Neurocomputing*, vol. 606, 2024, doi: 10.1016/j.neucom.2024.128284.

[10] X. Li, F. Ye, Y. Tian, and Y. Li, "Multi-head self-attention mechanism combined with feedforward network for time-varying nonlinear digital self-interference cancellation," *Digital Signal Processing*, vol. 155, 2024, doi: 10.1016/j.dsp.2024.104699.

[11] D. Nahavandi, R. Alizadehsani, A. Khosravi, and U. R. Acharya, "Application of artificial intelligence in wearable devices: Opportunities and challenges," *Comput Methods Programs Biomed*, vol. 213, p. 106541, Jan 2022, doi: 10.1016/j.cmpb.2021.106541.

[12] J. Ren, H. Li, A. Wang, K. Saho, and L. Meng, "Radar-based gait analysis by Transformer-liked network for dementia diagnosis," *Biomedical Signal Processing and Control*, vol. 91, 2024, doi: 10.1016/j.bspc.2024.105986.

[13] S. Tuli *et al.*, "AI augmented Edge and Fog computing: Trends and challenges," *Journal of Network and Computer Applications*, vol. 216, 2023, doi: 10.1016/j.jnca.2023.103648.

[14] E. V. Vijay and K. Aparna, "Deep Learning-CT based spectrum sensing for cognitive radio for proficient data transmission in Wireless Sensor Networks," *e-Prime - Advances in Electrical Engineering, Electronics and Energy*, vol. 9, 2024, doi: 10.1016/j.prime.2024.100659.

[15] H. Kautonen and A. A. Gasparini, "B-Wheel – Building AI competences in academic libraries," *The Journal of Academic Librarianship*, vol. 50, no. 4, 2024, doi: 10.1016/j.acalib.2024.102886.

[16] A. Kumar, N. Gaur, S. Chakravarty, M. H. Alsharif, P. Uthansakul, and M. Uthansakul, "Analysis of spectrum sensing using deep learning algorithms: CNNs and RNNs," *Ain Shams Engineering Journal*, vol. 15, no. 3, 2024, doi: 10.1016/j.asej.2023.102505.

[17] F. Obite, A. D. Usman, and E. Okafor, "An overview of deep reinforcement learning for spectrum sensing in cognitive radio networks," *Digital Signal Processing*, vol. 113, 2021, doi: 10.1016/j.dsp.2021.103014.

[18] A. B. K. Rabbi and I. Jeelani, "AI integration in construction safety: Current state, challenges, and future opportunities in text, vision, and audio based applications," *Automation in Construction*, vol. 164, 2024, doi: 10.1016/j.autcon.2024.105443.

[19] A. K. Saini, A. K. Yadav, and Dhiraj, "A Comprehensive review on technological breakthroughs in precision agriculture: IoT and emerging data analytics," *European Journal of Agronomy*, vol. 163, 2025, doi: 10.1016/j.eja.2024.127440.

[20] I. Kontorovich, "The road to "good" problems goes through initial responses to stimulating socio-mathematical situations," *The Journal of Mathematical Behavior*, vol. 73, 2024, doi: 10.1016/j.jmathb.2024.101135.

[21] A. Mendez, B. Prieto, I. F. J. M. Aguirre, and P. Sanmartin, "Better, not more, lighting: Policies in urban areas towards environmentally-sound illumination of historical stone buildings that also halts biological colonization," *Sci Total Environ*, vol. 906, p. 167560, Jan 1 2024, doi: 10.1016/j.scitotenv.2023.167560.

[22] G. Patra and S. Datta, "XAI for Society 5.0: Requirements, opportunities, and challenges in the current context," in *XAI Based Intelligent Systems for Society 5.0*, 2024, pp. 269-293.

[23] P. K. Pal and D. Kumar, "The coupled Kaplan–Yorke-Logistic map for the image encryption applications," *Computers and Electrical Engineering*, vol. 120, 2024, doi: 10.1016/j.compeleceng.2024.109850.

[24] V. Rodrigues, Z. Breda, and C. Rodrigues, "The implications of industry 4.0 for the tourism sector: A systematic literature review," *Heliyon*, vol. 10, no. 11, p. e31590, Jun 15 2024, doi: 10.1016/j.heliyon.2024.e31590.

[25] Y. Yang, Z. Yang, and Z. Yang, "Dynamic Jacobi graph and trend-aware flow attention convolutional network for traffic forecasting," *Digital Signal Processing*, vol. 141, 2023, doi: 10.1016/j.dsp.2023.104156.

[26] M. Rhiat *et al.*, "Maximizing solar energy efficiency: Optimized DC power conversion for resistive loads," *Computers and Electrical Engineering*, vol. 120, 2024, doi: 10.1016/j.compeleceng.2024.109867.

[27] B. Saoud, I. Shayea, A. E. Yahya, Z. A. Shamsan, A. Alhammadi, M. A. Alawad, and Y. Alkhrijah, "Artificial Intelligence, Internet of things and 6G methodologies in the context of Vehicular Ad-hoc Networks (VANETs): Survey," *ICT Express*, vol. 10, no. 4, pp. 959-980, 2024, doi: 10.1016/j.icte.2024.05.008.

[28] H. F. Nweke, Y. W. Teh, M. A. Al-garadi, and U. R. Alo, "Deep learning algorithms for human activity recognition using mobile and wearable sensor networks: State of the art and research challenges," *Expert Systems with Applications*, vol. 105, pp. 233-261, 2018, doi: 10.1016/j.eswa.2018.03.056.

[29] E. G. Acuña Acuña, "Assessment as a Fundamental Pillar in Engineering Education: Experiences in Research Projects," presented at the Proceedings of the 22nd LACCEI International Multi-Conference for Engineering, Education and Technology (LACCEI 2024): "Sustainable Engineering for a Diverse, Equitable, and Inclusive Future at the Service of Education, Research, and Industry for a Society 5.0.", 2024.

[30] A. Akhtarshenas, M. A. Vahedifar, N. Ayoobi, B. Maham, T. Alizadeh, S. Ebrahimi, and D. López-Pérez, "Federated learning: A cutting-edge survey of the latest advancements and applications," *Computer Communications*, vol. 228, 2024, doi: 10.1016/j.comcom.2024.107964.

[31] M. F. Munir, A. Basit, W. Khan, A. Saleem, A. Khaliq, and N. A. Baig, "Next-Gen solutions: Deep learning-enhanced design of joint cognitive radar and communication systems for noisy channel environments," *Computers and Electrical Engineering*, vol. 120, 2024, doi: 10.1016/j.compeleceng.2024.109663.

[32] K. Saing, H. H. Goh, D. Zhang, W. Dai, T. A. Kurniawan, and K. C. Goh, "Revolutionizing energy infrastructure: Automated route planning for underground transmission lines in Phnom Penh," *e-Prime - Advances in Electrical Engineering, Electronics and Energy*, vol. 9, 2024, doi: 10.1016/j.prime.2024.100633.

[33] S. S. Shijer, A. H. Jassim, L. A. Al-Haddad, and T. T. Abbas, "Evaluating electrical power yield of photovoltaic solar cells with k-Nearest neighbors: A machine learning statistical analysis approach," *e-Prime - Advances in Electrical Engineering, Electronics and Energy*, vol. 9, 2024, doi: 10.1016/j.prime.2024.100674.

[34] S. K. Yadav, B. Singh, and N. Mishra, "Real-time harmonics optimization of seven level converter for megawatt scale solar PV-utility integration," *e-Prime - Advances in Electrical Engineering, Electronics and Energy*, vol. 9, 2024, doi: 10.1016/j.prime.2024.100705.

[35] Z. Xu, Y. Cheng, Y. Qiao, Y. Wan, M. Shao, and C. Kang, "Adapting visible-light-image diffusion model for infrared image restoration in rainy weather," *Computers and Electrical Engineering*, vol. 120, 2024, doi: 10.1016/j.compeleceng.2024.109814.

[36] S. Sharif and A. Rahman, "Penetration and control of grid-forming (GFM) inverter in LFC of an enhanced IEEE 9-Bus interconnected power system," *Computers and Electrical Engineering*, vol. 120, 2024, doi: 10.1016/j.compeleceng.2024.109837.

[37] J.-H. Kim, "A study on the water content in distribution pole transformer using random forest model," *Computers and Electrical Engineering*, vol. 120, 2024, doi: 10.1016/j.compeleceng.2024.109823.